Robust Collocated Control of Large Flexible Space Structures

F. Angeletti*, P. Iannelli*, P. Gasbarri*, J. A. Perez Gonzalez**, N. Ellero***, T. Wattrelot***,
F. Ankersen****, M. Sabatini*, F. Celani*, G. B. Palmerini*

*Sapienza University of Rome, Rome, Italy (e-mail: paolo.gasbarri@uniroma1.it).

**Thales Alenia Space, Harwell, United Kingdom (e-mail: jose-alvaro.perez-gonzalez@thalesaleniaspace.com)

*** Thales Alenia Space, Cannes, France

**** European Space Agency (ESA-ESTEC), Noordwijk, Netherlands (e-mail: Finn.Ankersen@esa.int)

Abstract: Agile maneuvering and precise pointing control require special attention for spacecraft equipped with large flexible appendages. A joint academia-industry research involving Sapienza University of Rome, Thales Alenia Space in France and the European Space Agency (ESA), investigates the use of innovative solutions to counteract the deterioration in pointing accuracy stemming from interactions between a rigid bus and the flexible structures during operations. Specifically, this paper aims at presenting the design of an attitude/vibration control architecture in a μ-synthesis framework. The architecture consists of an attitude control system combined with a distributed network of actuators/sensors at structural level for active vibration control purposes. A spacecraft equipped with an interferometric Ka-band SAR payload and two solar arrays is considered as a useful and challenging benchmark problem to assess the proposed methodology. The numerical simulations, carried out via both a linearized setting and a nonlinear simulator, have proved the effectiveness of the robust collocated control in comparison with a baseline PID controller.

Keywords: Robust control, Large space structures, Active vibration control, collocated control

1. INTRODUCTION

Nowadays, spacecraft are demanded to fulfill increasingly precise requirements, which generally depend on strict pointing budget, maneuvering agility and on-board sensors and actuators. In this scenario, coupled interactions between structures' flexibility and spacecraft dynamics control, known as Control/ Structure Interaction (CSI) (Ketner (1989)) can significantly worsen spacecraft GNC performance, and even lead to instabilities and failures. Spacecraft with Large Space Structures (LSS) are generally characterized by very low damping and natural frequencies, which could hence easily overlap/interfere with the control bandwidth. Therefore, considering the spacecraft's flexibility in the control design phase is of utmost importance. At present, CSI issues relevant to LSS are solved at platform level, either by shaping GNC controllers for disturbance rejection or by designing control/structures frequencies separation. The most adopted control technique is the standard Proportional-Integral-Derivative (PID) controller, coupled with notch and roll-off filters for damping out the peaks of the main elastic modes (Bennani et Al. (2011)). Lately, alternative strategies to address the CSI problem have been considered, such as the implementation of distributed actuators/sensors on the flexible appendages to dampen out undesired elastic vibrations (Angeletti et Al. (2021)). Controllers which combine control/sensing devices at both platform and structural level are becoming more suitable to control applications, by tying together spacecraft flexible dynamics and control (Perez et Al.

(2016), Sabatini et Al. (2020), Hiramoto et Al. (2009)). This paper aims at giving a contribution on CSI applied to LSS by presenting the results of an industry-academia study funded by ESA[1]. A standard robust GNC platform architecture is enhanced by including a network of sensors and actuators on the spacecraft flexible appendages for vibration control. Pairs of sensors and actuators were set physically very close to each other which corresponds to the so-called collocated configuration. Such a configuration always leads to alternating poles and zeroes near the imaginary axis, which is translated into an unconditionally stable system (Preumont (2002)). The optimal location of distributed actuators/ sensors is investigated by using two in-parallel techniques for cross-check validation. The proposed control system combines measurements/actions from both the spacecraft hub and the devices distributed in the structures in a robust control setting.

The paper is organized as follows: Section 2 introduces the dynamics of the flexible spacecraft used as benchmarking problem in the ACACLAS study. The placement process of the collocated sensors/actuators network is also described. In Section 3, the design of the robust control and the synthesis results are discussed. Section 4 illustrates the controller performance in different space mission scenarios. Conclusions and future developments are finally presented.

2. SYSTEM MODEL

This section describes the case study. An overview of the spacecraft, named Satellite Testbed Affected By Large

---

Elasticity (STABLE), is shown in Figure 1. The spacecraft is composed of a central rigid body and three flexible appendages or subsystems (one payload and two solar arrays of 3x8m each). The payload, in turn, consists of two deployable booms (20m end-to-end length) and two reflectors (10m long) each placed at the end point of the booms. The proposed instrument concept is inspired by the Ka-band Radar Interferometer (KaRIn). To improve the generality of the study, two different types of structural elements have been considered: a beam structure (+Y-axis half of the payload mast), a truss structure (–Y-axis half of the payload mast and two reflectors backbone structure).
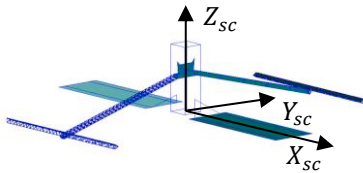

Figure 1. External overview of ACACLAS case study

2.1 Governing Equations of the Flexible Spacecraft

The spacecraft is divided into a rigid platform and flexible sub-structures, which are built in the MSC-NASTRAN suite and discretized in a rich finite element mesh (approximately 6000 nodes, 7000 elements). Data concerning the system mass, inertia, modes, and natural frequencies are imported in Matlab from NASTRAN to reconstruct the dynamic behavior of the structure. Thus, the nonlinear dynamic equations of the spacecraft are derived using a multibody approach (Alazard et Al. (2008)). The final governing equations can be expressed in matrix form (Iannelli et Al. (2021)). The properties of the system are listed in Table 1.

Table 1. Inertial properties

Main platform	
Mass	937.2 kg
Inertia matrix at platform CoM	$\begin{bmatrix} 591.6 & 2 & 4 \\ 2 & 625.2 & -7 \\ 4 & -7 & 549.6 \end{bmatrix}$ kgm^2
Payload (Mast inclination: 15°)	
Mass	443.2 kg
Inertia matrix wrt the CoM of the appendage	$\begin{bmatrix} 14680 & -0.3 & 0 \\ -0.3 & 1322 & -231.6 \\ 0 & -231.6 & 14890 \end{bmatrix}$ kgm^2
Solar Panels	
Mass	166.1 kg
Inertia matrix wrt the CoM of the appendage	$\begin{bmatrix} 152.4 & 0 & 6.8 \\ 0 & 1007 & 0 \\ 6.8 & 0 & 1158 \end{bmatrix}$ kgm^2

For the control synthesis, the assembled spacecraft governing equations are linearized around the Earth-pointing attitude, while the non-linear equations are implemented in the simulator to assess the performance of the controller in Sec. 4.

2.2 Collocated sensors and actuators

A key aspect of the ACACLAS study is related to the definition of the actuators/sensors network for active vibration control. Firstly, a trade-off is carried out to select the most promising sensing/actuating solution. Hence, PZT stacks are selected as actuators for STABLE due to their convenient forces/torques to mass ratio, their high bandwidth and higher technology readiness level. A (pi)-shaped piezoelectric stack actuator (P-PSA), mounted with a vertical offset with respect to the hosting structure, is here proposed (see Figure 2). The bending moment generated by P-PSA actuators on the controlled flexible structure is given by (Wei, Zhichun (2009)):

$$M = n \frac{d_{33} A_{pz} E_{pz}}{l_{pz}} h_a \psi_{act} \qquad (1)$$

where h_a is the distance between the actuator and the neutral plane of the passive structure, d_{33} the piezoelectric material coefficient, ψ_{act} is the actuation voltage, A_{pz}, E_{pz}, l_{pz} and n are the area, Young modulus, length and number of layers.
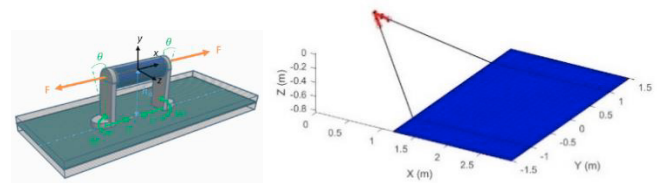

Figure 2: Left: Overview of the P-PSA stack actuator solution. Right: Solar Array FEM + actuators optimal locations (in red)

Regarding the sensing solution, piezo strain sensors were chosen in a collocated configuration with the P-PSA actuators. A charge amplifier is used to amplify the piezo sensors current signal to measurable output voltage used in the control loop. The sensors/actuators optimal placement in the LSS is investigated via two in-parallel methods for cross-check and validation:

- a norm-based method using controllability and observability gramians to define modal placement indices whose maxima indicate the optimal placement of sensors/actuators on the structure;
- a MSE/SVD method based on the inspection of the Modal Strain Energy (MSE) map and on the successive computation of Singular Values (SVDs) of the modal input matrix of the system.

The details of the above methods can be found in (Angeletti et Al. (2021)). For the sake of brevity, only the results of the collocated actuators/sensors placement on STABLE's solar arrays are reported in this paper. The optimal locations of the actuators/sensors to control/sense the first bending and torsional modes were identified on the yoke and near the attachment point to the main platform (see Figure 2). This result is coherently obtained via both inspecting the system gramians and MSE distribution map from the solar array finite element model. By using the same methodology, the placement process has been successfully carried out for the other substructures (i.e. payload beam, truss mast, and reflectors backbone structure) leading to a final actuators/sensors network composed of 11 pairs of piezo devices, included in the robust control design architecture.

3. ROBUST CONTROL

This section is devoted to introducing the design approach, synthesis process, and the stability/performance results of the proposed robust frame for the Advanced Collocated Active Control (ACAC), which combines the vibration/attitude controllers. As several system parameters are assumed to be uncertain, the system dynamic plant is recast in a Linear Fractional Transformation (LFT) representation (M-Δ) (Zhou, Doyle (1998)) to separate the uncertain/unknown part of the system from the known part, with the aim to carry out the robust synthesis operations. Further LFT model reduction procedures are also explored, as well as the selection of weighting functions to define the synthesis objectives and the implemented robust control algorithm.

3.1 Plant Structure for Robust Control Design

As a first step, STABLE LFT model is built by interconnecting in feedback a nominal plant (M) to a block-diagonal matrix $\Delta = diag(\Delta_i)$ with $||\Delta||_\infty \leq 1$. The synthesis model adopted to design the controller is presented in Figure 3.
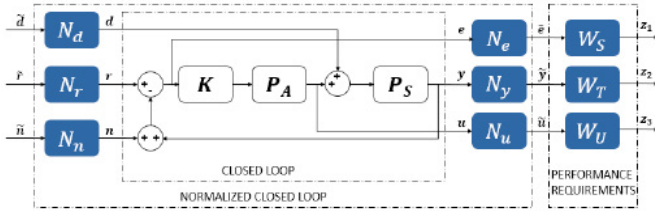

Figure 3. Schematics of synthesis model scheme

The closed loop inputs d, r, n indicate the external disturbance, reference signal and measurement noise vectors and $\tilde{d}, \tilde{r}, \tilde{n}$ are their normalized counterparts via the scaling functions N_d, N_r, N_n. The closed loop outputs e, y, u are respectively the error signal $e = r - y - n$, the measured output and control signals vectors, whereas $\tilde{e}, \tilde{y}, \tilde{u}$ are their normalized counterparts via the scaling functions N_e, N_y, N_u. Finally, z_1, z_2, z_3 are the performance outputs and W_S, W_T, W_U are the weighting functions. Block P_S represents the spacecraft system (both rigid and flexible parts) after removing the translation equations and neglecting the nonlinear terms. The input/output (I/O) signals of P_S are listed in Table 2. The model outputs are the measurements available for the closed loop control and the specific channels required to ensure the mission requirements on attitude error, relative torsion between the ends of the mast, Power Spectral Density (PSD) of the relative payload tip displacements (Table 2). Block P_A represents the actuators whose LFT model is composed of 14 inputs (3 torque inputs and 11 voltages for the distributed network of piezo-actuators) and 14 outputs (3 torque outputs and 11 actions exerted by the piezo-actuators on the flexible substructures). The actuators time delays are modelled with a Padé approximation with 1st order numerator and 5th order denominator. Uncertainties are only considered on the electro-mechanical parameter of the piezoelectric actuators, whilst no scattering on the time delay is assumed to avoid to complexify the full LFT model which is described in Section 3.2. The equivalent LFT model of the sensors and of the estimation is composed of two parts. The first part is composed of additive noises (band-limited white noise due to the GNC sampling frequency) to represent the navigation model based on star trackers and gyroscope data. The noise variance values considered in the synthesis process are $\sigma_{att} = 4$ arcsec and $\sigma_{rate} = 1$ arcsec/s for the spacecraft attitude and angular rate respectively. The second part represents the LFT models of the piezoelectric sensors considering the electro-mechanical part with uncertain parameters ($\pm 5\%$ of the nominal value).

Table 2. System I/O

Input	• 3-axis torque produced by the platform actuators (thruster or reaction wheel) • 11 actions of piezoelectric actuators located on appendages (Payload, Solar arrays)
Output	• 3-axis attitude of the spacecraft (vector part of the attitude quaternion) • 3-axis attitude rate of the spacecraft • 11 voltages of piezoelectric sensors located on appendages (Payload, Solar arrays). • relative angle (Torsion) between the two reflectors about Ysc-axis. • relative vertical displacement between the reflectors' centers (along Zsc-axis)

3.2 LFT Reduction

In the model in Section 3.1, the uncertainties are attributed to each substructure of the system in terms of both inertial and structural properties (natural frequencies and damping). Thus, the LFT synthesis model contains 91 uncertainties which are represented with Δ: 159x159, M: 196 inputs, 244 outputs and 163 states (without weighting functions). However, after performing preliminary robust control design using MATLAB Robust Control Toolbox, the synthesis process did not converge due to the complexity of the considered dynamic system in terms of the high number of uncertainties and system inputs/outputs. Therefore, model reduction techniques based on some assumptions and simplifications have been considered to guide the synthesis operations. The main actions are listed below:

1. Reduction of number of uncertainties: instead of introducing uncertainties to each spacecraft substructure, those are introduced in the inertial properties of the whole assembly. The assumed uncertainties in such Reduced Uncertainty Domain (RUD) are listed in Table 3.

2. Worst-case parameters selection: relevant variables are assumed to be known and equal to a worst-case scenario. For example, the actuation time delay is assumed as two samples periods, and flexible modes damping ratio is set to 0.01 for payload and 0.001 for solar arrays.

3. Reduction of repeated uncertainties for the flexible modes frequencies: it is well-known that the flexible modes of a structure can be modelled as second order systems. Consider, for example, the second order transfer function

$$R(s) = \frac{1}{s^2 + 2\xi\omega s + \omega^2} \qquad (2)$$

where $\omega = \omega_0(1 + \delta)$, ω_0 is the nominal frequency and $\delta \in [-a, a]$ is an uncertain parameter with a defining the desired maximum uncertainty. The minimal LFT model of $R(s)$ is composed of two occurrences of δ. Replacing ω^2

by $\omega_0^2(1 + (2 + a/2)\delta)$ a new LFT model composed of only one occurrence of δ is obtained.

Table 3. RUD System Uncertainties

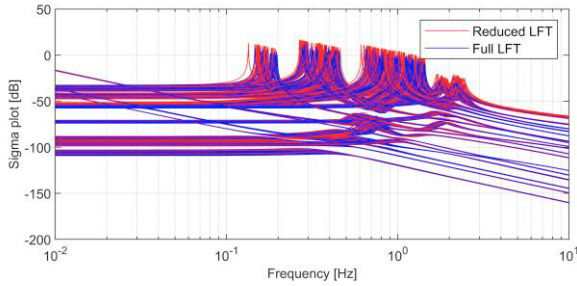| Quantity		Value
S/C Inertia	Diagonal terms	$\pm 2\%$
	Cross-diagonal terms	$\pm 20 kgm^2$
S/C Mass	Mass	$\pm 5\%$
S/C flexible modes (Natural frequencies)	Payload	$\pm 10\%$
	Solar Arrays	$\pm 20\%$
Piezo actuators	Electro-mechanical properties	$\pm 5\%$

Figure 4. Comparison between Reduced and Full LFT realizations (for each input/output pair)

A comparison between sampled Full and Reduced LFT realizations is shown in Figure 4. Note that the peaks of the Reduced LFT are higher than the ones in the full LFT model, resulting in a more conservative model for robust synthesis.

3.3 Robust Control Synthesis

The weighting functions are used to define the control design requirements by shaping the sensitivity, the complementary sensitivity and control sensitivity transfer functions. A diagonal structure is selected for all weighting functions as:

$$W_S^{ii}(s) = \left(\frac{\frac{s}{\sqrt[n]{M_S^{(i)}}} + \omega_S^{(i)}}{s + \omega_S^{(i)}\sqrt[n]{A_S^{(i)}}} \right)^{n_i}, W_T^{ii}(s) = \left(\frac{s + \omega_T^{(i)}\sqrt[n]{A_T^{(i)}}}{\frac{s}{\sqrt[n]{M_T^{(i)}}} + \omega_T^{(i)}} \right)^{n_i}$$

$$W_U^{ii}(s) = \left(\frac{\frac{s}{\sqrt[n]{M_U^{(i)}}} + \omega_U^{(i)}}{\frac{s}{\sqrt[n]{A_U^{(i)}}} + \omega_U^{(i)}} \right)^{n_i}$$

(3)

where the parameters $M_{\{S,T,U\}}^{(i)}, A_{\{S,T,U\}}^{(i)}, \omega_{\{S,T,U\}}^{(i)}$ are tunable quantities used to impose the required closed loop behaviour. The weight $W_S(s)$ in eq. (3) was chosen to shape the sensitivity function to enforce the following requirements:

- A minimum bandwidth of the closed loop system to satisfy minimum rise time requirements.
- A desired maximum overshoot of the response (generally below 30%) by constraining accordingly a value of the maximum peak of the sensitivity function via M_S.
- Desired steady state tracking error performance by constraining the low frequency gain of the sensitivity function through A_S.

Similar considerations are valid to shape the complementary sensitivity function via W_T, in response to reference and noise,

and the command sensitivity function via W_U, to guarantee compatibility with the considered actuation capabilities. In addition, other weighting functions were used to limit the torsion and vertical displacements of the payload mast. Figures 5 and 6 present respectively the singular values plots of the sensitivity, complementary sensitivity and control functions for the scaled closed loop system which are below the corresponding inverse of the performance weighting functions W_S, W_T, W_U.
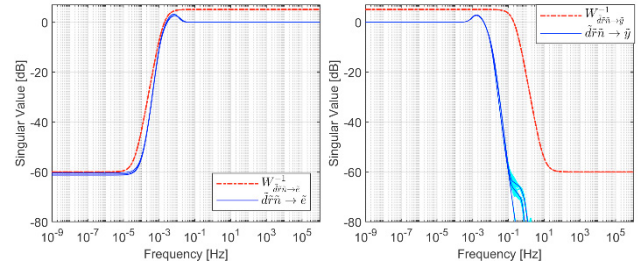

Figure 5. Left: Singular values of the sensitivity function Right: Singular values of the complementary sensitivity function
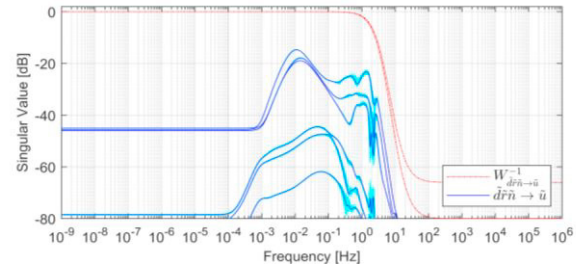

Figure 6. Singular values of the control function

Figures 7 presents the requirements for torsion and vertical displacements of the payload mast (in red) and the synthesis results (in blue). In both cases, the sigma plot shows that the transfers from inputs (i.e. noises, disturbances and references) to the payload outputs (i.e. relative torsion and relative displacement) satisfy the requirements.
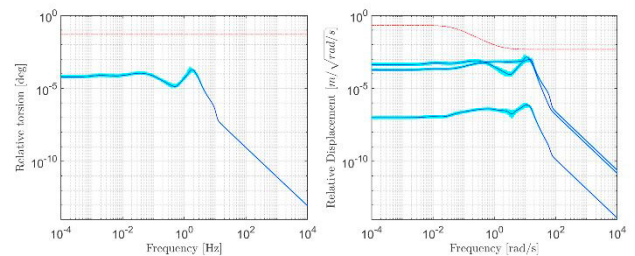

Figure 7. Left: Relative torsion between the two reflectors about Y_{sc}-axis. Right: Relative displacement between reflectors' centers

The lower and upper bounds of the μ-norm of the closed-loop system are computed as indicators for stability robustness. Figure 8 presents the results for a wide frequency region from 10^{-6} rad/s to 10^4 rad/s. The robust stability analysis leads to a peak value of 0.7, meaning that the closed-loop system is robust to the considered domain of uncertainties. Concerning robust performance, the analysis leads a peak

value of 0.9, meaning that the performance of the closed-loop system is robust to current uncertainties.

4. RESULTS

After completing the robust synthesis based on the linearized dynamics, the controller is tested on a non-linear simulator, which is also reproducing the orbital environment affecting the S/C. In this section, results are presented considering nominal pointing and Orbital Control Maneuver (OCM) scenarios.
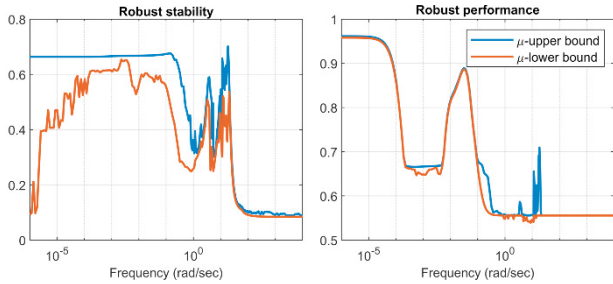
Figure 8: Left: μ-analysis Robust Stability (ACAC controller). Right: μ-analysis Robust Performance (ACAC controller)

The aim of the analysis is to demonstrate that the performance of the S/C – in terms of Attitude Pointing Error (APE) and tranquilization time - can be significantly improved by integrating the ACAC controller into the GNC architecture. To this purpose, a traditional PID controller is introduced as a benchmark for evaluating the performances of the combined attitude/ACAC one. Such baseline controller is composed of three decoupled PID controllers with roll-off filters (i.e. one PID controller with one filter per axis). The second order low pass filter (0.3 rad/sec bandwidth) eliminates high frequency signals and reduces the interaction with the appendages flexible dynamics.

4.1 Nominal Pointing

In this scenario the objective of the controller is to make the spacecraft follow a nominal nadir pointing (-Z_{sc} pointed towards the Earth and Y_{sc} across track) while rejecting disturbances coming from the environment (solar radiation pressure, drag and gravity gradient related to a 600 km LEO circular orbit) as well as internal vibrating sources. Figure 9 compares the pointing performance in term of APE temporal behavior for the PID and ACAC controllers for one orbital period. The analysis shows that the ACAC controller exhibits better performance in noise/disturbance rejection with respect to the baseline PID controller. This performance improvement is demonstrated also by evaluating the PSD of the APE in Figure 10 . Regarding the PID controller, the APE requirement is met in almost all frequencies except in the neighbours of 0.4 Hz, corresponding to the asymmetric solar array bending in the spacecraft XZ plane (located at 0.39 Hz). It is also present a slight non-compliance at 1.1 Hz, which corresponds to the symmetric bending of the solar arrays in the spacecraft XZ plane. On the other hand, Figure 10 (right) shows that the active vibration control components introduced in the system by the ACAC controller manages to counteract undesired elastic vibrations and consequently keep the PSD of the APE

under the specified requirements for the frequency range of interest. Additional tests on nominal pointing have been performed considering the transient disturbance generated by the thermal gradient originating from entering and leaving the eclipse zone (thermal snap). Such a disturbance provokes a sudden structural deformation of the flexible appendages greatly worsening the pointing of the spacecraft. In this scenario, the regular PID control exhibits a de-pointing transient when entering and leaving the eclipse zone due to the thermal snap disturbance. This transient can be seen in the APE profile shown in Figure 11. The transient event surpasses the limit imposed by the APE requirements around Y_{sc}. The transient worsens the pointing performance by a factor of 10 approximately, reducing the margins found for the nominal pointing scenario.
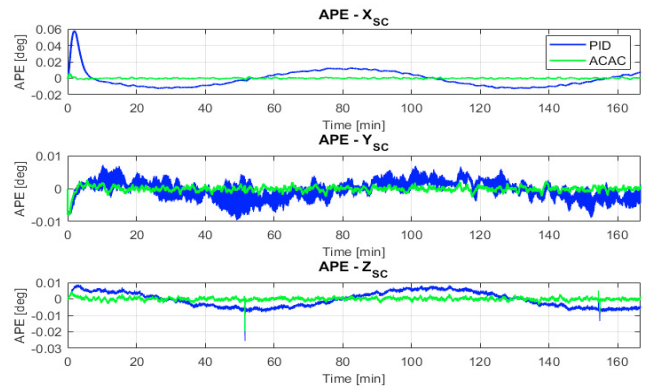
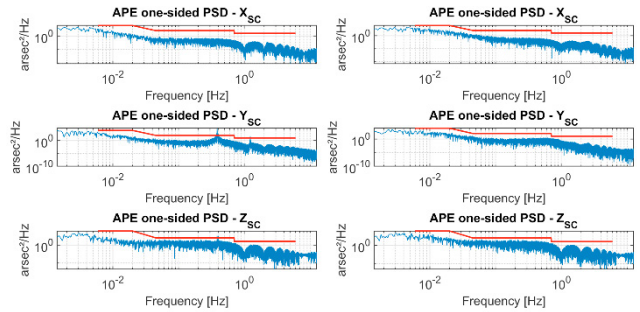Figure 9: APE temporal series for nominal pointing scenario

Figure 10: Left: PSD of the APE (nominal scenario with PID), Right: PSD of the APE (nominal scenario with ACAC). In blue the nominal performance, in red the requirement.
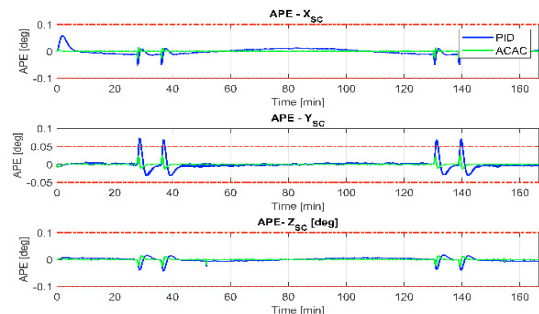
Figure 11: APE temporal series for nominal pointing scenario with thermal snap

When using the ACAC control, the thermal transient is substantially mitigated. As it can be seen in Figure 11, the APE overshoots are much lower than with baseline control and are kept within the requirements.

4.2 Orbital Control Maneuver (OCM) Scenario

In the orbit control manoeuvre scenario, a Δv manoeuvre is performed to increase or maintain spacecraft's altitude. Thus, a step force of 40 N is applied for approximately 2 min at the CoM along the $+Z_{sc}$ direction to inject the required Δv of 1 m/s. The objective of this test case is to evaluate the proposed control approach against sudden applied high forces which considerably excite the flexible structure. Figure 12 shows how the spacecraft with the standard PID control exhibits large de-pointing errors along the 3 axes during the Δv manoeuvre.
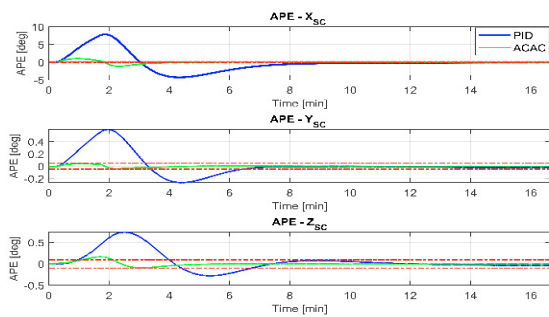

Figure 12: APE evolution during OCM manoeuvre for PID

Furthermore, the analysis has shown that the time needed to recover an attitude which satisfy the APE requirements (tranquilization time) is larger than 13 min. On the other hand, the ACAC controller achieves 80% improvement in the de-pointing error and tranquilization times lower than 3 min. Table 4 provides a summary of the ACAC performance compared to regular PID performance in terms of 3σ APE.

Table 4. Performance increase overview

Scenario	Performance increase of ACAC controller vs PID
Nominal pointing	- [81, 63, 77] % (increase of APE (3σ) along the 3 axes)
Thermal snap	- [80, 72, 59] % (increase of APE (3σ) along the 3 axes)
OCM (Δv)	- 80 % increase of APE performance - Tranquilization time >13 min (PID) - Tranquilization time < 3 min (ACAC)

The above results demonstrate the advantages of the ACAC approach. Indeed, the improvement in pointing performance is one order of magnitude higher with respect to the PID baseline controller. In addition, the ACAC controller leads to reducing the transients due to slews and the recovery time after OCM.

5. CONCLUSIONS

The paper presented the design of an attitude/vibration control architecture in a μ-synthesis framework. The proposed architecture consists of an attitude control system combined with a distributed network of actuators/sensors at structural level for active vibration purposes. A very large flexible spacecraft equipped with an interferometric Ka-band SAR payload and two solar arrays is considered. Four different scenarios have been used to verify and validate the proposed controller, and to demonstrate the advantages of embedded active control of spacecraft flexible modes through collocated actuators. The simulation scenarios have covered nominal pointing with and without thermal snap, large angle slew and Δv manoeuvre. Numerical simulations, carried out via a nonlinear orbital simulator, showed better performances of the robust control in comparison to a baseline PID controller. In the future, an extensive Monte-Carlo campaign will be performed to assess the conservativism that the reduced model causes. The proposed ACAC controller will be employed in an experimental platform floating on a frictionless plane simulating the dynamics of a large flexible structure to verify experimentally the effectiveness of the approach.

REFERENCES

Alazard, D., et Al. (2008). Linear Dynamic Modeling of Spacecraft with Various Flexible Appendages and On-board Angular Momentums, *7th Inter. ESA Conference on GN&C Systems*, June 2008 - 5 June 2008 (Tralee, Ireland)

Angeletti, F., et Al.. (2021). End-to-end design of a robust attitude control and vibration suppression system for large space smart structures, *Acta Astr.*, Vol. 187, 2021, 416-428,

Bennani, S., Ankersen, F. et Al. (2011). Robust Attitude Control Design for the BIOMASS Satellite (Earth Explorer Core Mission Candidate). *IFAC Proc.,* Vol. 44, 5130-5135.

Hiramoto, K., et Al. (2009). Integrated Design of System Parameters, Control and Sensor Actuator Placement for Symmetric Mechanical Systems, *In 48th IEEE Conference on Decision and Control*, Shanghai, China, Dec. 2009

Iannelli, P., Angeletti, F., Gasbarri, P. (2021). Model-Based FDI Applied to a Piezoelectric Active Vibration Suppression System for Smart Flexible Spacecraft. *Aerotec. Missili Spaz*. Vol. 100, 147–160

Ketner, G.L. (1989). Survey of historical incidents with Control-Structures Interaction and recommended technology improvements needed to put hardware in space, *Control Structures Interaction Office*, NASA-LARC, 1989.

Perez J.A. et Al. (2016). Integrated Control/Structure Design of a Large Space Structure using Structured H_∞ Control, *20th IFAC Symp. on Automatic Control in Aerospace*, Vol. 49, Issue 17, 302-307

Preumont, A. (2002). *Vibration control of active structures* Kluwer, Dordrecht.

Sabatini M., Palmerini G.B., Gasbarri P. (2020). Synergetic approach in attitude control of very flexible satellites by means of thrusters and PZT devices, *Aerospace Science and Technology*, Vol. 96, 2-11

Wei W, Zhichun Y. (2009) A compact piezoelectric stack actuator and its simulation in vibration control *Tsinghua Sci. Technol.*, Vol.14, Issue S2, 43-48

Zhou, K., Doyle, J. (1998). *Essentials of robust control* Prentice Hall, Upper Saddle River.